



Available online at [www.sciencedirect.com](http://www.sciencedirect.com)



Reliability Engineering and System Safety 00 (2014) 1–21

Reliability  
Engineer-  
ing &  
System  
Safety

## Coupling mode-destination accessibility with a quantitative seismic-risk assessment to identify at-risk communities

Mahalia Miller<sup>a</sup>, Jack W. Baker<sup>a</sup>

<sup>a</sup>*Stanford University, Stanford, CA USA*

---

### Abstract

In this paper, we develop a framework for coupling mode-destination accessibility with a quantitative seismic-risk assessment to identify communities at a high risk for travel disruptions after an earthquake. For a case study of the San Francisco Bay Area, we find that accessibility varies more strongly from location to location than between income classes, and we identify particularly at-risk communities. We also observe that communities more conducive to local trips by foot or bike are predicted to be less impacted by losses in accessibility.

© 2014 Published by Elsevier Ltd.

**Keywords:** Infrastructure, Risk, Earthquakes

---

**1. Introduction**

Seismic risk assessment in earthquake engineering tends to focus on buildings, bridges, and the performance of infrastructure systems. For measuring the performance of transportation systems, researchers typically use engineering-based metrics such as the post-earthquake connectivity loss, which quantifies the decrease in the number of origins or generators connected to a destination node [e.g., 1], or the post-earthquake travel distance between two locations of interest [e.g., 2]. These frameworks have provided insight into seismic vulnerability and possible risk mitigation. However, the link to the human ramifications can be limited.

In the field of vulnerability sciences, researchers have long stressed the importance of the impact on human welfare from earthquakes. For example, Bolin and Stanford write that, “‘Natural’ disasters have more to do with the social, political, and economic aspects than they do with the environmental hazards that trigger them. Disasters occur at the interface of vulnerable people and hazardous environments” [3]. A recent World Bank and United Nations report echoed this idea that the effects on human welfare turn natural hazards into disasters [4].

Historical events emphasize the complex social effects of earthquakes. For example, on one hand the 1994 Northridge earthquake caused major damage to nine bridges, which, while significant, represented only 0.5% of the bridges estimated by Caltrans to have experienced significant shaking [5]. On the other hand, over half of businesses reported closing after the earthquake with 56% citing the “inability of employees to get to work” as a reason [6]. Furthermore, the total economic cost of transport-related interruptions (“commuting, inhibited customer access, and shipping and supply disruptions”) from this earthquake is estimated at 2.16 billion USD (2014) [7], using the consumer price index to account for inflation.

An emergent trend in earthquake engineering is estimating the cumulative extra time needed for travel after a simulated future earthquake, sometimes called travel time delay [e.g., 8, 9]. This performance measure captures basic

re-routing due to road closures and enables identifying roads more likely to be very congested. Travel time approximately measures one aspect of the impact on people, but does not capture the fact that some destinations and trips have higher value than others. Furthermore, this approach measures the impacts by focusing on aggregate regional effects rather than individual communities and demographic groups. Some recent work has looked at other metrics, such as the qualitative criteria-based metric “disruption index” [10]. However, this does not provide a quantitative link between the technical impact and the human ramifications. Other work has looked at resiliency, but defined it in pure engineering terms, such as percentage of a simplified road network that is functional [11]. Outside of transportation systems, some researchers have investigated the interplay between earthquake damage, such as damage to the electric power and wastewater networks, and the usability of houses and other buildings; this represents an important first step [12].

In contrast to the work on transportation-related seismic risk, urban planning has a long tradition of studying the impact on people of events and policy [13]. Accessibility is one metric popular in urban planning to measure the impact of different transportation network scenarios, and it measures how easily people can get to desirable destinations, which is one measure of social impact [14]. Within urban planning, accessibility has been measured in many ways, including individual accessibility, economic benefits of accessibility, and mode-destination accessibility [15]. The mode-destination accessibility is computed by taking the log value of the sum of a function of the utilities of each destination over all possible destinations and travel modes, where the utility decreases if getting to that destination is more costly or time-intensive [16]. This choice of accessibility definition is particularly applicable to quantifying the impacts of catastrophes, such as earthquakes, because certain destinations might be more critical for people in certain locations or from different socio-economic groups (such as low income or high income). However, this accessibility measure has not yet been linked to risk assessment. In addition, the majority of work to date assumes that travel demand and mode choice will remain unchanged after a future earthquake, which historical data suggests is not the case [7]. A first step towards considering variable demand is work in the literature that varies demand by applying a constant multiplicative factor on all pre-earthquake travel demand [8].

In this paper, we develop a framework for coupling mode-destination accessibility with a quantitative seismic-risk assessment to identify at-risk populations and measure the accompanying impacts on human welfare. We illustrate our approach with a case study of the San Francisco Bay Area transportation network, including highways, local roads, and public transportation lines. This study analyzes a set of forty hazard-consistent earthquake scenarios, ground-motion intensity maps, and damage maps, as we introduced in [17] using the optimization procedure we proposed in [18]. For each of these damage maps, we model damage with a practical, agent-based transportation model used by the local transportation authorities that includes damage to bridges, roads, and transit lines, and varies demand. Then, with this model, we estimate the predicted losses in accessibility according to 12 socio-economic groups used by local planners for the case study region, based on income class, and ratio of personal vehicles to workers in a household.

## 55 2. Case study: San Francisco Bay Area

### 56 2.1. Case study overview

We focus on the San Francisco Bay Area, a seismically-active region, to illustrate our approach (Figure 1). The area follows a polycentric metropolitan form, with San Francisco as the primary center and other jobs concentrated in suburban centers, such as Silicon Valley [19]. The region has a wide array of trip patterns for mandatory and non-mandatory trips. Furthermore, trip times and routes vary greatly depending on travel preferences and workplace locations [19]. Thus, we might expect noticeable disparities between households in the risk of travel time delays due to earthquakes.

This analysis considers the complex web of roads and transit networks of the case study area. The roads are modeled by a directed graph  $G = (V, E)$ , where  $V$  is a finite set of vertices representing intersections, and the set  $E$ , whose elements are edges representing road links, is a binary relation on  $V$ . In this model,  $(|V|, |E|) = (11,921, 32,858)$  including centroidal links and  $(|V|, |E|) = (9,635, 24,404)$  without. Centroidal links do not correspond to particular physical roads but instead capture more subtle travel flows, such as from outside the study area or the flow of people to and from some minor local roads. We also in 43 transit networks, as detailed in [17].

We model damage from ground shaking intensity to a set of 1743 highway bridges impacting the road and some transit networks, with data provided by the California Department of Transportation (Caltrans), and 1409 structures



Figure 1. Study area: San Francisco Bay Area, CA with specific travel analysis zones (TAZs) used in the case study marked in blue.

71 impacting the rapid transit network, BART, with data provided by that agency. We refer readers to [17] for more  
 72 details about matching these structures, hereafter called components, to the relevant road and transit networks.

### 73 2.2. Ground-motion intensity maps

#### 74 2.2.1. Theory

75 We now describe how to produce a set of maps with ground-motion intensity realizations at each location of interest,  
 76 and corresponding occurrence rates that reasonably capture the joint distribution of the ground-motion intensity.  
 77 First, we generate  $Q$  earthquake scenarios from a seismic source model. The seismic source model specifies the  
 78 rates at which earthquakes of specified magnitudes, locations, and faulting types will occur. This set of earthquake  
 79 scenarios is comparable to a stochastic event catalogue in the insurance industry.

80 Second, for each earthquake scenario in the seismic source model, we use an empirical ground-motion prediction  
 81 equation (GMPE) [e.g., 20, 21, 22, 23] to model  $Y$ , the resulting intensity measure at each location of interest [e.g.,  
 82 25].

83 Then, for each of the  $Q$  earthquake scenarios, we sample  $b$  realizations of the spatially-correlated ground-motion  
 84 intensity residual terms. Readers are referred to [26] for a survey of sampling methods. Once residuals are sampled,  
 85 the total log ground-motion intensity ( $Y$ ) is computed as

$$\ln Y_{ij} = \overline{\ln Y(M_j, R_{ij}, V_{s30,i}, \dots)} + \sigma_{ij}\epsilon_{ij} + \tau_j\eta_j \quad (1)$$

86 where  $j$  is the ground-motion intensity map index ( $j = 1, \dots, m$  where  $m = Q \times b$ ),  $\epsilon_{ij}$  is the normalized within-event  
 87 residual in  $\ln Y$  representing location-to-location variability and  $\eta_j$  is the normalized between-event residual in  $\ln Y$   
 88 and the other parameters are defined above. Both  $\epsilon_{ij}$  and  $\eta_j$  are normal random variables with zero mean and unit  
 89 standard deviation. The vector of  $\epsilon_{ij}$  can be modeled by a spatially-correlated multivariate normal distribution [e.g.,  
 90 27] and the  $\eta_j$  by a standard univariate normal distribution.

91 The result is a set of  $m$  ground-motion intensity maps (e.g., Figure 2(a)). Since we simulate an equal number  
 92 ( $b$ ) of ground-motion intensity maps per earthquake scenario, the annual rate of occurrence for the  $j^{th}$  ground-motion  
 93 intensity map is the original rate of occurrence of the earthquake scenario, divided by  $b$ . We denote the rate associated  
 94 with the  $j^{th}$  ground-motion intensity map as  $w_j$ .

#### 95 2.2.2. Implementation

96 To generate a stochastic catalog of ground-motion intensity maps, we use the OpenSHA Event Set Calculator [28].  
 97 This software outputs the mean,  $\ln Y_{ij}$ , and standard deviation values,  $\sigma_{ij}$  and  $\tau_j$ , for all locations of interest for a  
 98 specified seismic source model and ground-motion prediction equation, which are needed inputs for Equation 1. The  
 99 intensity measure is the 5%-damped pseudo absolute spectral acceleration ( $Sa$ ) at a period  $T = 1s$ , which is the  
 100 required input to the fragility functions below. This spectral acceleration value represents the maximum acceleration  
 101 over time that a linear oscillator with 5% damping and a period of 1 second will experience from a given ground  
 102 motion. We calculate these values at each component location (bridges and other structures). Using one ground-  
 103 motion intensity measure per component is a common simplification of the time-varying acceleration dynamics [e.g.,  
 104 29, 9] that may have lower errors for components with a natural period near 1 second as opposed to long-span bridges.  
 105 We use the UCERF2 seismic source model [30], Wald and Allen topographic slope model for the shear wave  
 106 velocity  $V_{s30,i}$  [31], and the Boore and Atkinson [20] ground-motion prediction equation. We simulate the ground-  
 107 motion intensity maps by combining the mean terms from the Event Set Calculator and spatially-correlated residual  
 108 terms of the ground-motion intensity (using [27]) according to the basic ground-motion model (eq. 1).

### 109 2.3. Damage maps

#### 110 2.3.1. Theory

111 Calculating network performance risk requires assessing the structural damage of relevant components after future  
 112 earthquakes. The link between ground-motion intensity and structural damage is often provided by *fragility functions*.  
 113 Fragility functions express  $P(DS_i \geq ds_i | Y_{ij} = y)$ . We assume one component, such as a bridge, per site location, so we  
 114 will identify both components and site locations via the index  $i$ . Using that notation,  $DS_i$  is a discrete random variable  
 115 whose value represents the damage state for the  $i^{th}$  component and  $ds$  is a damage state threshold of interest. The  
 116 damage state is conditioned on a realization,  $y$ , of the random variable  $Y_{ij}$ , the ground-motion intensity at the  $i^{th}$  site

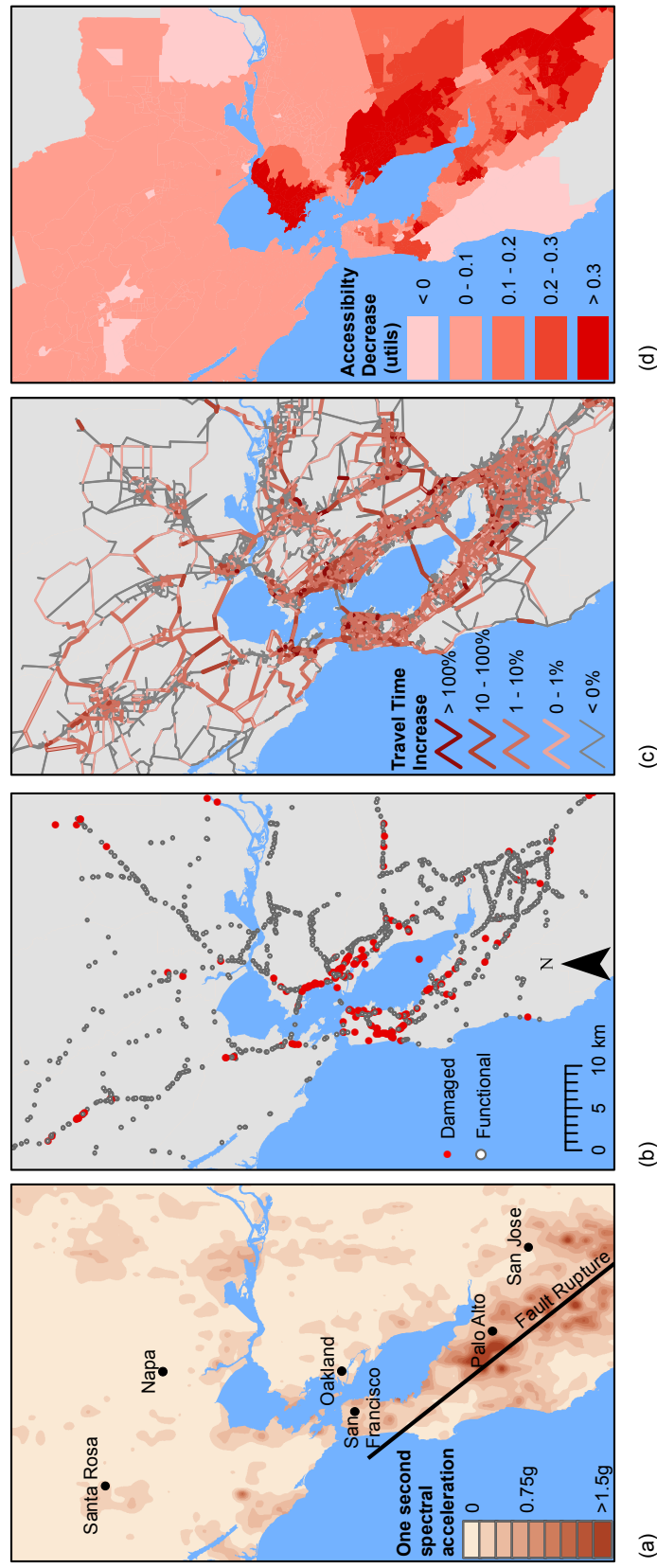


Figure 2. Illustration of the risk framework for one earthquake event including a) One-second spectral acceleration (ground-motion intensity) map with earthquake rupture, b) bridge (component) damage map, c) map of travel time increase (network-performance measure) values, and d) map of accessibility values averaged over all market segments by travel analysis zone (TAZ).

and  $j^{th}$  ground-motion intensity map. Researchers have calibrated fragility functions using historical post-earthquake data [e.g., 32], experimental and analytical results [e.g., 33], hybrid approaches, and expert opinion. It is possible to sample the damage states from a joint distribution that includes correlation, such as due to similarities in design or construction practices [e.g., 34].

By sampling a damage state for each component, with probabilities obtained from the fragility functions given the ground-motion intensity, we produce a damage map (e.g., Figure 2(b)). The damage map has a realization of the damage state of each relevant component. This sampling process can be repeated multiple times to simulate multiple damage maps per ground-motion intensity map. For example, if equal numbers of damage maps are sampled per ground-motion intensity map ( $c$  damage maps per ground-motion intensity map), the weight of the  $j^{th}$  damage map should be adjusted accordingly to  $w_j$ , where  $w_j = \frac{w_j}{c}$ , and  $j' = 1, \dots, J$ .

*Functional percentage* relationships link the component damage to the functionality of network elements. For example, in a road network, when a bridge collapses, the traffic flow capacity of the road it carries and it crosses can be modeled as reduced to zero. These relationships are typically derived from a combination of observation and expert opinion, often due to data scarcity [35]. Furthermore, the relationships are typically deterministic for a certain component damage state and restoration time [35]. Thus, in this paper, each damage map corresponds to a functionality state for every element of the network.

### 2.3.2. Implementation

*Component damage.* For the case study, we use fragility functions of the following form to provide the link between ground-motion shaking and component damage:

$$P(DS_i \geq ds_S | Y_{ij} = y) = \Phi\left(\frac{\ln y - \lambda_{\varsigma,i}}{\xi_{\varsigma,i}}\right), \quad (2)$$

where  $\Phi$  is the standard normal cumulative distribution function,  $\lambda_{\varsigma,i}$  and  $\xi_{\varsigma,i}$  are respectively the mean and standard deviation of the  $\ln Y_{ij}$  value necessary to cause the  $\varsigma^{th}$  damage state to occur or be exceeded for the  $i^{th}$  component, and the other variables are defined above. By using the previous equation and the inverse method, we can sample realizations of component damage states for a given ground-motion intensity.

The California Department of Transportation (Caltrans) provided the fragility function values  $\lambda_{\varsigma,i}$  and  $\xi_{\varsigma,i}$  used in this study for the highway components in summer 2012, which was last updated in 2007 and includes various retrofitted bridges [36]. The  $\lambda_{\varsigma,i}$  values are based on component characteristics including number of spans and age as detailed in [32]. The  $\xi_{\varsigma,i}$  values are given as a constant. The BART seismic safety group provided the fragility function values  $\lambda_{\varsigma,i}$  and  $\xi_{\varsigma,i}$  used in this study for the BART-related components for the state of the network in summer 2012. Data is available for the aerial structures, primarily in the East Bay, but not tunnel data. These correspond to the safety performance goals under the recent retrofit program [37]. The numbers are comparable to the Caltrans fragility data. For the BART components, however,  $\xi_{\varsigma,i}$ , the standard deviation of the  $\ln S_a$  value necessary to cause the extensive damage state to occur or be exceeded, varies depending on the component. Both sets of fragility functions are based on the assumption that damage can be reasonably accurately estimated by the ground motion intensity at each site independently, and that the damage state can be reasonably estimated by an analytical model considering a single ground-motion intensity measure. In addition, the fragility curves do not directly consider the effects of degradation. Current work is ongoing to refine these assumptions [e.g., 33, 38, 39].

Per ground-motion intensity map, we sample 1 damage map (e.g., Figure 2(b)), which has a realization of the component damage state at each component location according to the fragility function (eq. 2). The provided fragility functions do not consider correlation of the structural capacities, but other models could be used [e.g., 34].

*Transit network damage.* Each of the 43 transit systems we considered will be impacted differently. For Caltrain, conversations with managers suggest that given that there is one shared track system, the system would either be fully operational or not at all. Similarly, managers suggested modeling the VTA system as fully functional or not. Depending on where the BART train cars are when the earthquake strikes, the agency could accommodate different emergency plans. However, BART representatives suggested considering that if any part of a route is damaged, the entire corresponding route would not be operational (but other routes on different tracks might be still operational). In other words, each BART route as well as the Caltrain and VTA routes are each a weakest-link system, so the failure

163 of a single component will cause the route to be non-operational. We modeled the ferry systems as fully functioning  
 164 for all earthquake events. For all earthquake events including the baseline, trans-bay and cross-county bus lines were  
 165 discontinued, but main lines in urban areas as well as other local bus networks were maintained per recommendations  
 166 from the MTC, though they may face delays due to modeled traffic congestion.

167 *Road network damage.* Each component damage state maps directly to the traffic capacity on associated road seg-  
 168 ments. We use a functional percentage relationship to compute the traffic capacity of relevant road segments. Based  
 169 on discussions with Caltrans, we consider travel conditions one week after an earthquake, since it is a critical period  
 170 for decision making. For example, one week after most events, bridges should have been inspected and surface dam-  
 171 age should be repaired, but major reconstruction would not have yet begun. According to our functional percentage  
 172 relationship, at this point in time, the components have one of two classes of functionality, zero traffic capacity and  
 173 full traffic capacity [35]. We can thus summarize the component damage using two damage states  $ds_s$ ,  $ds_{damaged}$  and  
 174  $ds_{functional}$ , which correspond to the common HAZUS *extensive* or *complete* damage states and the *none*, *slight*, or  
 175 *moderate* damage states respectively [35]. Thus, the functional percentage relationship assigns zero traffic capacity  
 176 on road segments that have at least one component in the  $ds_{damaged}$  damage state, and full traffic capacity otherwise.  
 177 We do not consider network damage from sources other than main structural damage from ground shaking, such as  
 178 tunnel displacement or liquefaction, but the framework allows including such considerations.

#### 179 2.4. Network performance

##### 180 2.4.1. Theory

181 The final step for the event-based risk analysis is to evaluate the network performance measure,  $X$ . For this  
 182 application, we consider a metric popular in urban planning, *mode-destination accessibility change* [e.g., 15, 41, 42]  
 183 (e.g., Figure 2(d)). Mode-destination accessibility, hereafter referred to as accessibility, measures the distribution of  
 184 travel destination opportunities weighted by the composite utility of all modes of travel to those destinations, i.e.,  
 185 the ease of someone getting to different destinations weighted by how desirable those destinations are [16, 14]. The  
 186 utility function for the mode-destination choice may be estimated using a multinomial random utility model where  
 187 the logsum represents the accessibility value [43, 16, 14]. Namely, accessibility for a particular agent  $a$  is

$$Acc_a = \ln \left[ \sum_{v \in C_a} \exp(V_{a(c)}) \right], \quad (3)$$

188 where  $V_{a(c)}$  is the utility of the  $c^{th}$  choice for the  $a^{th}$  person for  $a = 1, \dots, A$ , and  $C_a$  is the choice set for the  $a^{th}$   
 189 person [16]. Choices refer to travel destinations and the mode of travel (driving, walking, bus, etc.). The units are a  
 190 dimensionless quantity, *utils*. As an extension, the accessibility values from the previous equation can be converted  
 191 into equivalent time and dollar amounts using *compensating variation* for cost-benefit studies; for the case study,  
 192 0.0134 *utils* (generic measure of utility) equals the value of one minute per day [14, 44, 45] and we conservatively  
 193 value one hour of time as approximately \$15 [46]. In other words, one *util* is worth approximately \$20 per person per  
 194 day based on these assumptions. With nearly 7 million people in the region, even small changes in *utils* lead to large  
 195 economic losses. Since accessibility measures how easily people can get to the destinations they desire, accessibility  
 196 is used as one of the measures of human welfare [e.g., 14].

197 Once the accessibility network performance measure is computed for each damage map, we aim to estimate the  
 198 exceedance rate of different levels of performance. The annual rate,  $\lambda$ , of exceeding some threshold of network  
 199 performance is estimated by summing the occurrence rates of all damage maps in which the performance measure  
 200 exceeds the threshold:

$$\lambda_{X \geq x} = \sum_{j'=1}^J w_{j'} \mathbb{I}(X_{j'} \geq x) \quad (4)$$

201 where  $x$  is an accessibility value threshold of interest and  $X_{j'}$  is the accessibility value realization for the  $j'^{th}$  damage  
 202 map. The variable  $w_{j'}$  is the occurrence rate of the  $j'^{th}$  damage map. The indicator function  $\mathbb{I}$  evaluates to 1 if the  
 203 argument,  $X_{j'} \geq x$ , is true, and 0 otherwise. By evaluating  $\lambda$  at different threshold values, we derive an exceedance  
 204 curve (e.g., Figure 6).

Income class	Income range, 1989 USD	Income range, 2014 USD
Low	0 - \$25,000	0 - \$47,334
Medium	\$25,000 - \$45,000	\$47,334 - \$85,202
High	\$45,000 - \$75,000	\$85,202 - \$142,004
Very high	more than \$75,000	more than \$142,004

Table 1. Income class definitions for the case study region, as defined by the local planning organization, the MTC [45] and also translated to current 2014 USD using the consumer price index.

#### 205 2.4.2. Implementation

206 We compute accessibility using *Travel Model One* (version 0.3), an activity-based model used by the Metropolitan  
 207 Transportation Commission (MTC), the local metropolitan planning organization (MPO) [47]. It represents the full  
 208 road network as well as the public transit networks, biking, and walking. Travel demand data consists of the locations  
 209 of different households in the case study area, their destination preferences and utilities, their number of vehicles, and  
 210 their income and other demographic data [47, 45]. More details can be found in [48]. This data was collected by  
 211 the MTC from surveys and census information. We assume that the distributions of travel preferences do not change  
 212 after an earthquake, although the actual destinations and trips may vary. For example, if a trip takes a very long time  
 213 after a simulated earthquake, it is less likely that the trip will occur. The result is a *variable* travel demand model.  
 214 This model uses a combination of Java code called CT-RAMP [49], and the CitiLabs Cube Voyager and Cube Cluster  
 215 software programs, which are part of a leading commercial software suite for transportation planning [47]. This model  
 216 differs from previous representations of this network [e.g., 9, 50], since it includes not only major roads but also local  
 217 roads and transit lines. We have provided further details about computing mode-destination accessibility using this  
 218 high-fidelity model in [17].

219 This analysis considers 40 interesting and hazard-consistent events, as defined by 40 sets of ground-motion in-  
 220 tensity maps, damage maps, accessibility performance measure realizations, and corresponding annual rates of oc-  
 221 currence. We selected this set of events with the optimization-based procedure we introduced in [18]. Readers are  
 222 referred to [17] for more details about this set of events.

223 In the following sections, we first compare region-wide results, and then focus on particular characteristics of  
 224 three communities (Figure 1 shows the study area and three communities). Finally, we discuss generalizable trends.

### 225 3. Results and Discussion

#### 226 3.1. Overview of results region-wide

227 In this section, we analyze region-wide trends in accessibility losses for the case study area. We first analyze  
 228 each of the 12 socio-economic groups used in practice for the case study region [45]. These socio-economic groups  
 229 correspond to all combinations of four different income classes (Table 1), and three different classes of automobile  
 230 availability in the household (zero automobiles, fewer automobiles than household members that work, a greater or  
 231 equal number of automobiles as compared to the number of household members that work).

232 We first assess the data availability for each of the segments. Each data point represents a trip by a person of a  
 233 household, who is modeled as an agent in the high-fidelity transportation model. The results suggest comparing house-  
 234 holds with at least one car, because for households without cars (no cars), only the low income class has reasonably  
 235 many trips.

236 General patterns emerge in the expected losses in accessibility. The expected losses are computed by taking  
 237 an average of the accessibility results for each of the 1454 travel analysis zones (TAZ) for each earthquake event,  
 238 weighted by the adjusted annual likelihood of occurrence from the optimization results.

239 First, we notice that the ratio of cars to the number of people who work in a household is correlated with accessi-  
 240 bility risk; a higher ratio corresponds to higher expected decreases in accessibility. This corresponds to going across a  
 241 column in Figure 3. For example, for the first row representing low income households, we notice a marked change in  
 242 accessibility across the columns, as indicated by an expanded area of darkened TAZs from left to right (Figure 3(a-c)).  
 243 Note that 1 *util* corresponds to a consumer value of compensating variation of approximately \$20 per person per day,  
 244 which assumes low (conservative) estimates of the value of time for travel delays and value of getting to destinations.

245 We might expect these households with more cars to take longer trips because there might be a relationship  
 246 between needing to travel longer distances and needing an extra car or two in a household. This is indeed the case,  
 247 but it is not fully predictive. In fact, there is only a weak trend between average trip length for a TAZ before any  
 248 earthquake and the predicted impact on accessibility (Figure 4). Instead, we hypothesize that there are other latent  
 249 variables correlated with car ownership. For example, the geographic distribution of people without cars varies.  
 250 Additionally, in Section 3.5, we will further explore the correlation between the percentage of car-based trips and  
 251 accessibility risk. We will show that TAZs with fewer car-based trips tend to have lower risk of accessibility losses.

252 Second, controlling for car ownership, we see a fairly equitable distribution of risk across income class segments.  
 253 For example, by looking at households with fewer workers than cars (middle column of Figure 3), the variation from  
 254 TAZ to TAZ is significantly more striking than the difference across income segments (Figure 3(b,e,h,k)). Similarly,  
 255 while trip lengths are slightly longer for higher income households, the differences are subtle.

256 Thus, for a given TAZ, the differences across incomes are not that great. At the same time though, there is  
 257 an unequal geographic distribution of wealth in the San Francisco Bay Area. Because of this, when we aggregate  
 258 accessibility risk across TAZs, we see that accessibility risk rises with increasing household income (Figure 6(b)).  
 259 Therefore, even though the poor are generally the most vulnerable to natural disasters including hurricanes, floods  
 260 and earthquakes, wealthier households in the San Francisco Bay area are more vulnerable than the other income  
 261 groups to earthquake-related accessibility risk.

262 Next, we consider which geographic parts of the San Francisco Bay Area are at an elevated risk. The results show  
 263 regions of high risk: in the East Bay due East of San Francisco, in the suburbs of San Jose, along the coastal and  
 264 Bay-side regions South of San Francisco (Millbrae and Pacifica, e.g.), and in parts of San Francisco (South-Central  
 265 neighborhoods including Westland Highlands and Glen Park neighborhoods). One may have expected more high risk  
 266 areas on the San Francisco Peninsula, because of the San Andreas fault, which can generate large magnitude events.  
 267 In contrast, the East Bay has higher shaking levels at more moderate return periods, due to the higher relative annual  
 268 frequency of events on the Hayward Fault; this is correlated to bridge damage and thus road closures. Furthermore,  
 269 the data suggests that both the more common moderate-magnitude East Bay events and the rare higher-magnitude  
 270 San Andreas events can cause accessibility problems for the East Bay. Figure 5 shows one sample realization of a  
 271 M6.85 Hayward event and one sample realization of a M7.45 San Andreas event—both follow the general trend of  
 272 high predicted accessibility losses in the East Bay. In contrast, while any events could contribute to the risk in San  
 273 Francisco, our model results show the main accessibility losses in San Francisco corresponding to the San Andreas  
 274 events. Figures 5(c,d) provide one such example. Figures 5(e,f) show an example of a lower magnitude event farther  
 275 away from the main population centers, a M6.35 event in the Great Valley Pittsburg-Kirby Hills Fault. This shows  
 276 how the range of more minor faults in the East Bay can contribute to that area's risk. Also, we have shown the results  
 277 for one socio-economic group in Figure 5, but the other socio-economic groups follow the same general patterns,  
 278 albeit with different specific values.

279 Finally, we can examine the rates of loss exceedance (eq. 4). Figure 6 shows a similar shape to the loss exceedance  
 280 curves for other metrics such as portfolio losses and travel time delay [17]. Note that the results are primarily valid  
 281 in the 100 to 2475 year return periods, since this is the range chosen for the map selection optimization problem.  
 282 Recognizing that the impact varies significantly by TAZ, as indicated by Figure 3, we also examine the accessibility  
 283 loss exceedance curve for three communities: part of the San Francisco financial district, Danville, and Pacifica  
 284 (Figure 1). These correspond to TAZ IDs 2, 1161, and 224 respectively. This part of the San Francisco financial  
 285 district represents an area with relatively low expected changes in accessibility (Figure 3), whereas Danville and  
 286 Pacifica are at an elevated risk in almost all socio-economic groups (Figure 3). The general trends are corroborated by  
 287 the loss exceedance curves for these three communities (Figure 6(a) shows an example for the socio-economic group  
 288 with medium income households with fewer cars than workers). In other words, the average middle-class person from  
 289 Danville in a household with fewer cars than people who work is expected to experience travel-related losses up to 1  
 290 *utils* per day after a rare earthquake, which he or she values at approximately \$20 per day considering a conservative  
 291 estimate of travel time and destination value. In contrast, his or her fellow Bay Area resident in San Francisco has  
 292 expected losses of only a tenth as much as experienced by a Danville resident. At return periods greater than 100  
 293 years, we notice that Danville and Pacifica follow a similar general pattern, which differs dramatically from that of  
 294 San Francisco.

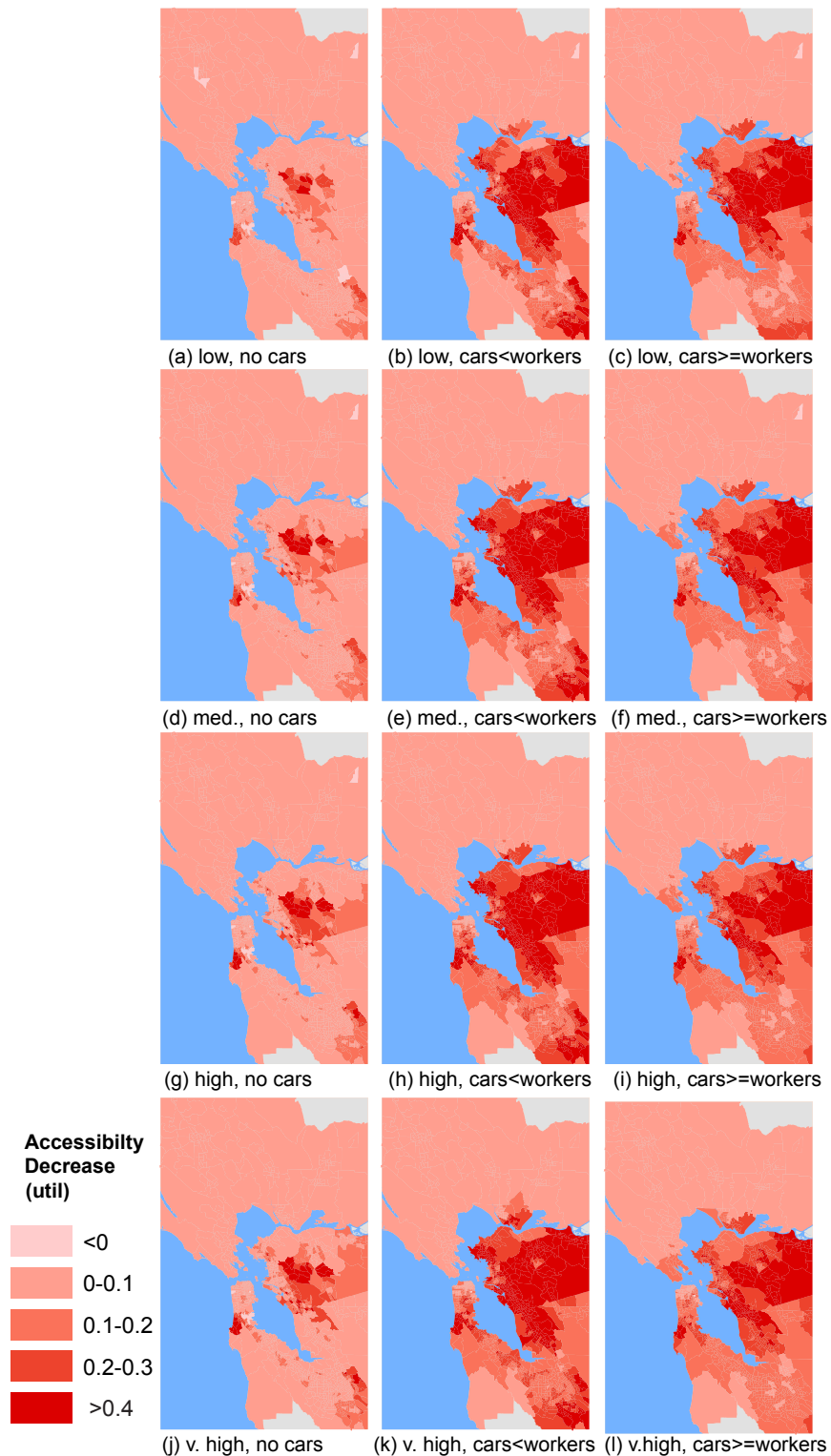


Figure 3. Expected changes in accessibility per person per day for each combination of income class and car ownership group. The darker the color, the greater the losses in accessibility.

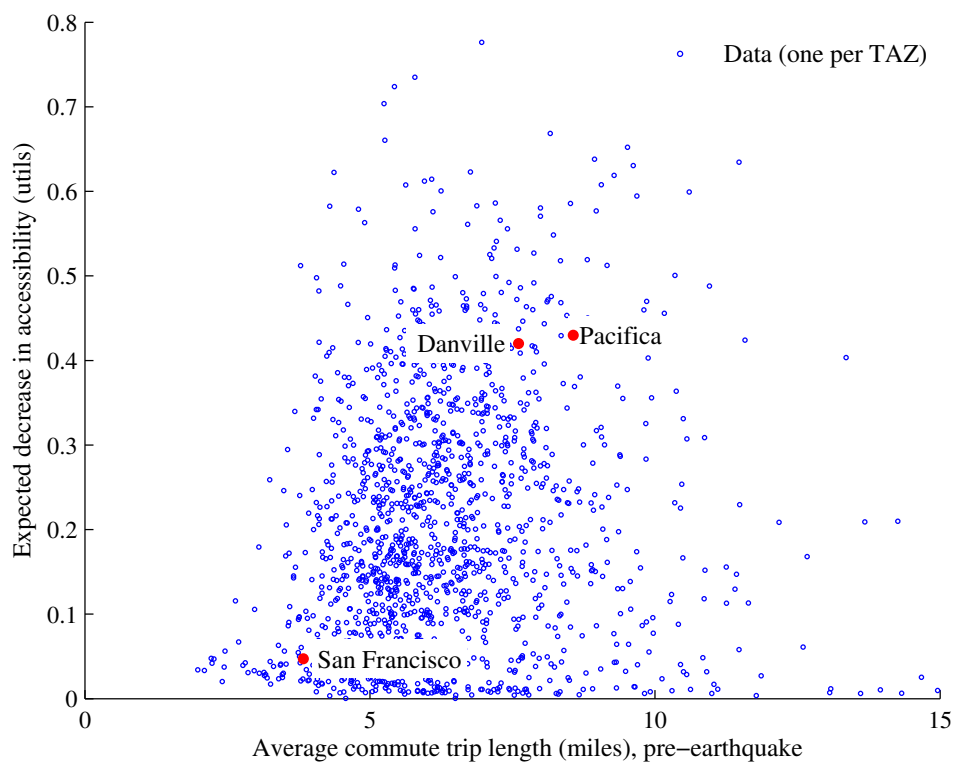


Figure 4. Trip length (pre-earthquake) versus change in total accessibility per person per day. Each dot represents data from one TAZ, and red dots highlight the data points for the three case study communities: San Francisco financial district, Danville, and Pacifica.

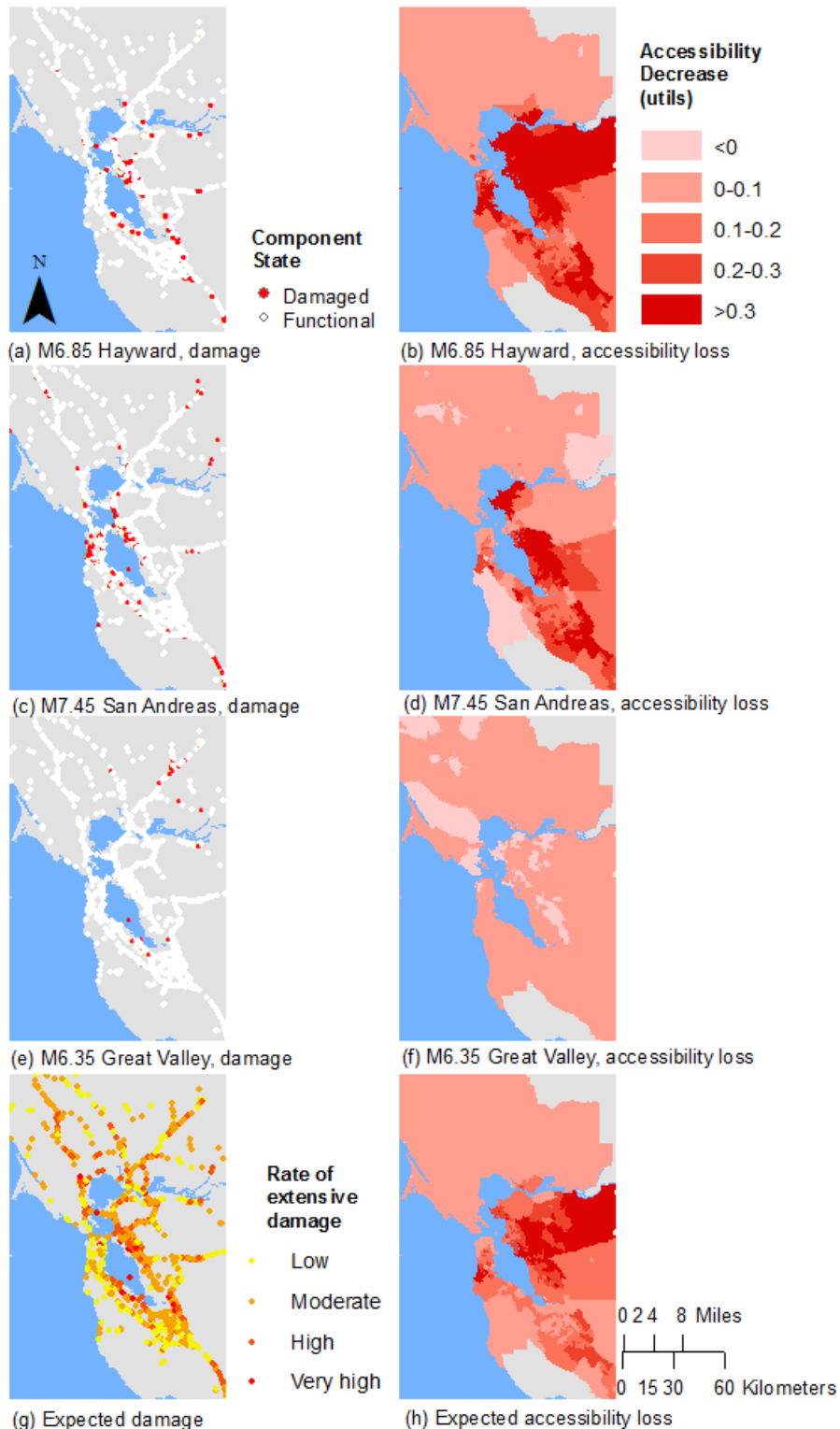


Figure 5. Bridge damage (red = damaged) and corresponding accessibility losses per person per day by TAZ for medium income households with fewer cars than workers. The bottom row has expected values calculated as a weighted average over all events.

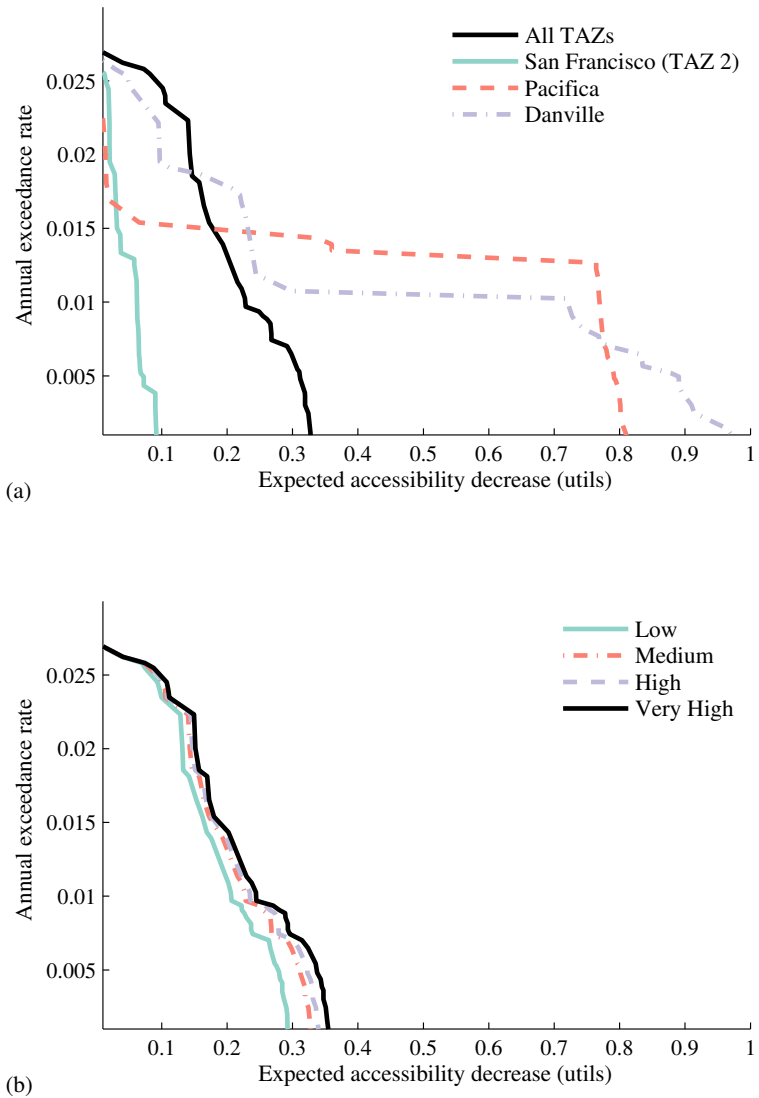


Figure 6. Accessibility annual loss exceedance curve with a comparison by (a) case study TAZs and average over all TAZs and (b) income class; all curves are in *utils* per person per day for medium income households with fewer cars than workers .

295 *3.2. Analysis for San Francisco, CA financial district*

296 In this section, we will explore some possible explanations for why this San Francisco TAZ (Figure 1) has lower  
 297 expected accessibility losses than most other communities. First, the financial district of San Francisco differs dramatically  
 298 from many other TAZs in that the percentage of trips made by car is relatively small (38% versus an average of  
 299 85% across all TAZs). Households traveling by foot or bike will be less influenced by network damage, because the  
 300 model considers only damage to the road network and transit systems; thus, foot travel routes and travel times will not  
 301 be affected in this model. We also observe that more trips by foot and bike correspond to destinations that are closer  
 302 geographically. The impact of travel mode shift post-earthquake will be further explored in Section 3.5.

303 Second, the average time for a trip to and from work is about average for a TAZ in this region and also follows  
 304 a similar distribution to that of the other TAZs; the average trip distance for trips is only 7% lower than the average  
 305 for all trips region-wide. Since the trip time and length are relatively typical, but the accessibility is much lower than  
 306 average, the trip time and length do not explain the differences in accessibility losses.

307 In summary, the data suggests that a major cause for the low expected accessibility impact for the financial  
 308 district of San Francisco is the lower relative dependence on cars for mobility. In the next section, we will contrast  
 309 the San Francisco example with results from Pacifica, another Peninsula community that, nonetheless, is expected to  
 310 be at high risk of losses in accessibility.

311 *3.3. Analysis for Pacifica, CA*

312 We might not suspect that Pacifica, CA would be at an extremely elevated risk of accessibility losses across most  
 313 market segments, as compared to other communities, because it is not unusually close to a major earthquake fault.  
 314 In addition, the percentage of pre-earthquake car-based trips is around average for the case study area (88% versus  
 315 an average of 85%). In contrast to most other regions, however, Pacifica is wedged between the Pacific Ocean to  
 316 the West and the coastal mountains to the East. Indeed, the main access road is California Highway 1, which has  
 317 various vulnerable bridges included in the case study dataset. There are no viable alternative routes on local roads.  
 318 Since almost all trips are by car from Pacifica and the average trip length is much longer than the region-wide average  
 319 (108% longer), the road issue is particularly serious.

320 As a comparison, consider the next main town along the Pacific coast, Half Moon Bay, about 13 miles South. Half  
 321 Moon Bay has significantly lower expected accessibility losses compared to Pacifica (0.11 *utils* per day for a person  
 322 in Half Moon Bay in middle income household with fewer cars than workers, given an event in the dataset, versus  
 323 0.43 *utils* per day for a similar person in Pacifica). While the seismic hazard is similar, the population is about one  
 324 third the size, so there is less demand for the limited road capacity [51]. Furthermore, and likely most significantly,  
 325 Half Moon Bay has a key alternative to California Highway 1, California Highway 92, which links to Silicon Valley  
 326 and the main highways of that region (US-101 and I-280). Our results indicate that since Pacifica, CA is unusually  
 327 reliant on one road with key vulnerabilities for access, it has an elevated risk for losses in accessibility.

328 *3.4. Analysis for Danville, CA*

329 We will first examine the trip length characteristics for Danville, CA. The distribution of pre-earthquake commute  
 330 trips from Danville, CA is shifted towards both longer distance and longer time than the communities we have studied  
 331 so far; for example, the average length of a trip from Danville is 85% longer than the average over all trips originating  
 332 from any TAZ. More specifically, there is a relatively higher proportion of trips taking 60–74 minutes and traveling  
 333 over 40 miles than in the other communities. The consequence of these longer trips is more opportunities to be  
 334 impacted by a road closure, simply because more roads and bridges will be used. Moreover, the road layout near  
 335 Danville, CA mandates many highway trips, which increase the likelihood of crossing bridges; bridges are the part of  
 336 the network for which we model the vulnerability.

337 Next, we look at patterns of expected bridge damage. Bridge damage is important for many regions, including  
 338 Danville, because the percentage of car-based trips is high (85% of all trips on average, and also 85% of Danville-  
 339 origin trips). For damage map realizations for the three earthquake events we introduced—M6.85 Hayward Fault,  
 340 M7.45 San Andreas Fault, M6.35 Great Valley Fault—some bridges in the Oakland area are in the extensive or  
 341 greater damage state (Figure 5(a,c,e)). These correspond to bridge closures in the model. In addition, in the first two  
 342 cases, there are closures to the north of Danville, which represents one of the two main travel routes from Danville.  
 343 There are also scattered closed bridges to the west of Danville, a top travel corridor for people of Danville because of

Functionality	BART	Caltrain	Muni Light Rail	VTA Light Rail
Full	3	13	25	9
50-99%	10	0	15	0
1-49%	8	0	0	0
None	19	27	0	31

Table 2. Transit network functionality as a count out of the forty simulated events for BART, Caltrain, Muni Light Rail, and VTA Light Rail. Functionality is measured by the percentage of lines that are operational given a damage map (based on a ground-motion intensity map).

the workplace centers in San Francisco, Oakland, and Silicon Valley (all to the west). As for transit, in the first two events, all BART lines are closed, so there are limited alternatives to the popular road routes. The result is that the residents of Danville, CA have reduced access to their normal destinations after all these events.

We can also look at bridge damage in a probabilistic event-set-based manner. The expected damage over all events represents the annual rate of a bridge being in the extensive or complete damage state for an extensively-sampled, hazard-consistent set of 113,940 damage maps (Figure 5(g)). This figure indicates that bridges in the Oakland-Berkeley area are particularly likely to be damaged. We also see a few high likelihood bridges to the North of Danville. Thus, the data suggests that the relative position of high-risk bridges to Danville contributes to this community's accessibility risk.

### 3.5. Impact of travel mode shifts and regional variations in travel mode patterns

First, we compare patterns of transit system damage with patterns of travel mode shifts after earthquake events. Over all the simulated events, taking a weighted average by the annual likelihood of each event, we see a reduction in transit ridership (25% weighted average decrease from the base case). This is not surprising. The heavy rail systems (BART and Caltrain) are not fully operational in most of the forty simulated events (Table 2), and these have heavy ridership. The light rail systems (VTA and Muni light rail) also suffered losses in many events (Table 2). The result is an average increase in the percentage of trips by the other modes (foot, car, and bike).

A notable exception is the M6.35 Great Valley, Pittsburg-Kirby Hills Fault earthquake event, as illustrated in Figure 5(e,f). In this event, there were no line closures on the major transit systems (BART, Caltrain, Muni, and VTA Light Rail). There were, however, some bridge closures on the highways (Figure 5(e)). The result was a slight increase in transit ridership and also in trips by foot.

In general, accessibility impact grows with increasing number of damaged transit lines, particularly in combination with high numbers of damaged bridges (Figure 7). The results do not conclusively show that transit is a key contributor to accessibility risk, but based on individual examples, the data suggests this conclusion. For example, in the set of forty events analyzed with the high-fidelity model, the M6.85 Hayward Rogers-Creek and the M7.45 Northern San Andreas Fault event both have a similar number of damaged bridges (around 11%); these are noted by points A and B respectively in Figure 7. These correspond to the bridge damage and accessibility maps in Figures 5(a,b) and 5(c,d) respectively. However, this Hayward Rogers-Creek event has significantly higher accessibility impact. Similarly, the transit impact was different. This Northern San Andreas event had only 4 of the 14 BART lines, all Caltrain, and all VTA Light Rail lines not operational, whereas this Hayward Rogers-Creek event had all 14 of the 14 BART lines, all Caltrain, all VTA Light Rail and 3 of the 8 Muni light rail lines not operational. Thus, the Hayward Rodgers-Creek event featured significantly higher losses to the transit network. Moreover, the differences in accessibility results could not have been predicted from simpler models focusing on bridge portfolio losses, because the percent of damaged bridges was about the same, and the San Andreas event actually corresponded to a greater increase in fixed-demand travel time.

Second, we examine the correlation between a community's walkability, as measured by the percentage of total trips made by that travel mode, and the expected decrease in accessibility by community. We see that an increased percentage of pre-earthquake trips on foot corresponds to a lower average decrease in accessibility (Figure 8). This result corroborates the specific example of the San Francisco Financial District we saw in Section 3.2. Furthermore, on average, the number of by-foot trips slightly increases after the earthquake events where road congestion worsens. This model result is consistent with the observations after the 1995 Kobe earthquake, in which many commuters switched to walking and biking ("non-mechanized modes") in the weeks after the earthquake [7]. In conclusion, the

<sup>385</sup> data suggests that TAZs, i.e. communities, which have a greater walkability are also more resilient to earthquake-  
<sup>386</sup> related accessibility risk.

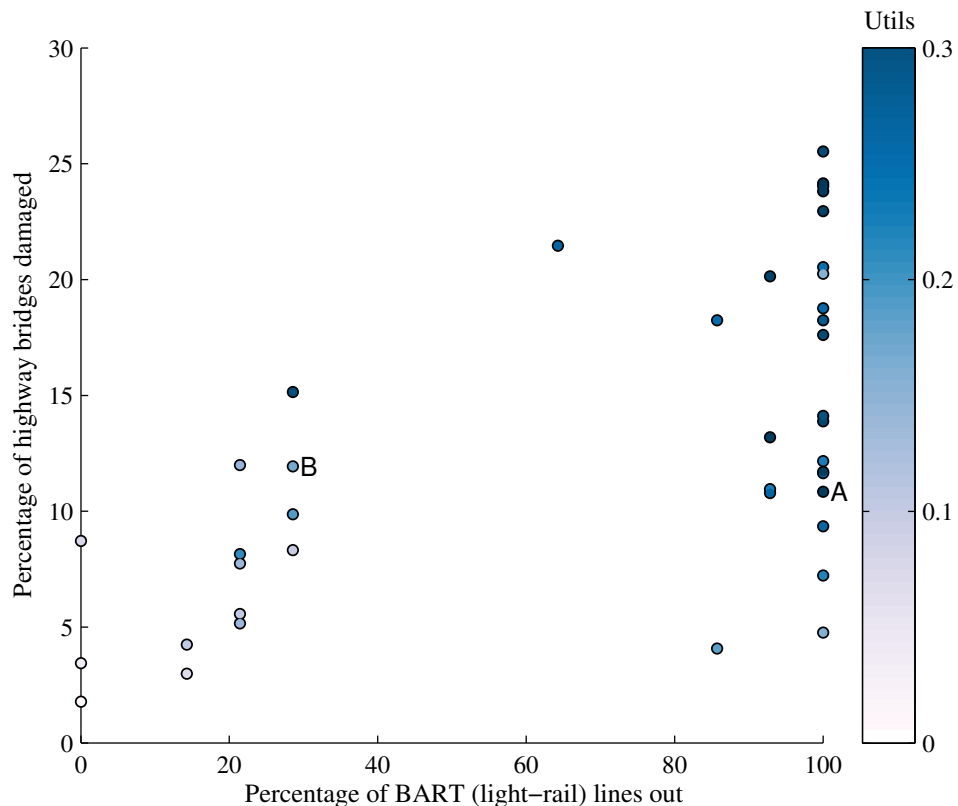


Figure 7. Percentage of BART (heavy-rail) lines not operational versus percentage of highway bridges damaged, where each data point corresponds to one earthquake damage map. The values are color-coded by the average loss in accessibility per day per person over all TAZs for households with the fewer cars than people who work. Two events discussed in this section are marked by the letters A and B.

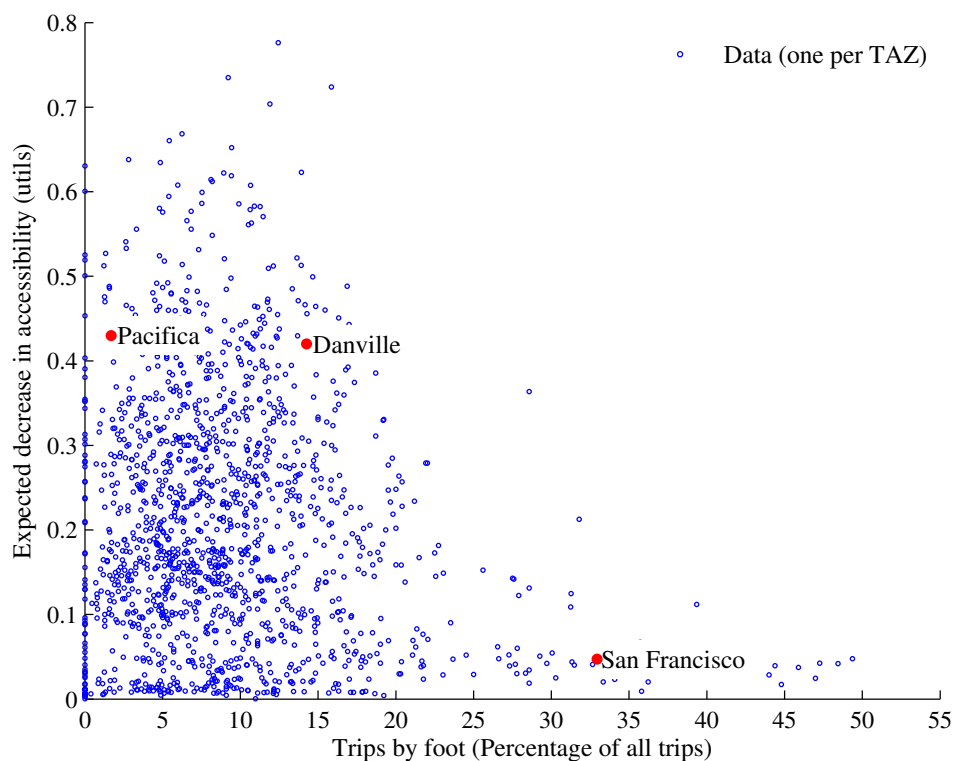


Figure 8. Percentage of total trips by foot (pre-earthquake) versus decrease in total accessibility, measured in *utils* per day (for households with the number of cars less than the number of workers). Each dot represents data from one TAZ, and red dots highlight the data points for the three case study communities: San Francisco financial district, Danville, and Pacifica.

387 **4. Conclusions**

388 Here we have shown how mode-destination accessibility links post-earthquake infrastructure damage to the impact  
 389 on human welfare and enables identifying at-risk geographic and demographic groups in a region. Adopting this  
 390 state-of-the-art performance metric from the urban planning community, we have illustrated its use for seismic risk  
 391 assessment and mitigation through a case study of the San Francisco Bay Area. For the case study, we consider a  
 392 set of 40 hazard-consistent earthquake scenarios, ground-motion intensity maps, damage maps, and corresponding  
 393 annual rates of occurrence. For each damage map, we processed the data for analysis in a high-fidelity, activity-based  
 394 travel model that includes the road network, transit networks, walking and biking options, variable travel demand, and  
 395 mode choice. We used this data and model to compute the mode-destination accessibility, a performance measure for  
 396 each community and each socio-economic group (defined by income class and car ownership).

397 We saw stark differences in accessibility from location to location. Specifically, we found that areas in the suburbs,  
 398 such as the far East Bay, South San Jose and select communities just south of San Francisco, were particularly at risk.  
 399 We found that these geographic trends persisted across income classes and car ownership groups. Nonetheless, on  
 400 average, higher income households with more cars than workers had the highest risk across the studied socio-economic  
 401 groups. One key reason is the geographic clustering of these households in higher-risk areas. Another factor is that  
 402 these households tend to take longer daily trips, thus crossing more roads and bridges and possibly increasing the  
 403 likelihood of disruption.

404 This study also demonstrated that travel modes shift after an earthquake, and communities who can more easily  
 405 make these adjustments are generally predicted to experience lower post-earthquake losses in accessibility. The results  
 406 suggest that the walkability of a community, as measured by the percentage of pre-earthquake trips by foot, is closely  
 407 linked to reduced accessibility risk. We also found that in almost all of the simulated earthquake events, the transit  
 408 system, particularly the heavy rail (BART and Caltrain) lines, is predicted by this model to be severely impacted. The  
 409 result is a reduced mode share for transit and increased trips by the other modes (car, walk, and bike). Thus, this study  
 410 suggests that not including transit can lead to an nonconservative estimate of seismic risk of transportation systems.  
 411 The model shows, however, that when transit is not damaged—which is very rare for this case study—ridership  
 412 increases.

413 In conclusion, mode-destination accessibility offers important applications for further investigation into the impact  
 414 to human welfare of engineering losses and mitigation efforts. This work lays the foundation for future work in risk  
 415 mitigation and policy to reduce the vulnerability of at-risk communities. It also suggests that initiatives making  
 416 communities more conducive for cycling and walking to work can increase resiliency.

417 **References**

- 418 [1] L. Dueñas-Osorio, J. I. Craig, B. J. Goodno, Seismic response of critical interdependent networks, *Earthquake Engineering & Structural*  
   419 *Dynamics* 36 (2) (2007) 285306. doi:10.1002/eqe.626.
- 420 [2] S. E. Chang, M. Shinozuka, J. E. Moore, Probabilistic earthquake scenarios: Extending risk analysis methodologies to spatially distributed  
   421 systems, *Earthquake Spectra* 16 (3) (2000) 557–572. doi:10.1193/1.1586127.
- 422 [3] R. C. Bolin, L. Stanford, *The Northridge earthquake: vulnerability and disaster*, Routledge, London; New York, 1998.
- 423 [4] The World Bank and the United Nations, *Natural hazards, unnatural disasters: the economics of effective prevention*, Tech. rep., The World  
   424 Bank, Washington D.C. (2010).
- 425 [5] California. Dept. of Transportation. Post Earthquake Investigation Team, *Northridge earthquake, 17 January 1994: PEQIT report*, California  
   426 Department of Transportation, Division of Structures, Sacramento, 1994.
- 427 [6] K. J. Tierney, Business Impacts of the Northridge Earthquake, *Journal of Contingencies and Crisis Management* 5 (2) (1997) 87–97.  
   428 doi:10.1111/1468-5973.00040.
- 429 [7] P. Gordon, H. W. Richardson, B. Davis, Transport-related impacts of the Northridge earthquake, National Emergency Training Center, 1998.
- 430 [8] A. Kiremidjian, J. Moore, Y. Y. Fan, O. Yazlali, N. Basöz, M. Williams, Seismic risk assessment of transportation network systems, *Journal*  
   431 *of Earthquake Engineering* 11 (3) (2007) 371–382. doi:10.1080/13632460701285277.
- 432 [9] N. Jayaram, J. W. Baker, Efficient sampling and data reduction techniques for probabilistic seismic lifeline risk assessment, *Earthquake*  
   433 *Engineering & Structural Dynamics* 39 (10) (2010) 1109–1131. doi:10.1002/eqe.988.
- 434 [10] C. S. Oliveira, M. A. Ferreira, F. M. d. S., The concept of a disruption index: application to the overall impact of the July 9, 1998 Faial  
   435 earthquake (Azores islands), *Bulletin of Earthquake Engineering* 10 (1) (2012) 7–25. doi:10.1007/s10518-011-9333-8.
- 436 [11] P. Bocchini, D. M. Frangopol, Restoration of bridge networks after an earthquake: Multicriteria intervention optimization, *Earthquake Spectra*  
   437 28 (2) (2012) 426–455. doi:10.1193/1.4000019.
- 438 [12] F. Cavalieri, P. Franchin, P. Gehl, B. Khazai, Quantitative assessment of social losses based on physical damage and interaction with infrastruc-  
   439 tural systems, *Earthquake Engineering & Structural Dynamics* 41 (11) (2012) 1569–1589. doi:10.1002/eqe.2220.
- 440 [13] F. S. Chapin, *Urban land use planning*, University of Illinois Press, 1970.

- [441] [14] D. A. Niemeier, Accessibility: an evaluation using consumer welfare, *Transportation* 24 (4) (1997) 377396.
- [442] [15] K. T. Geurs, B. van Wee, Accessibility evaluation of land-use and transport strategies: review and research directions, *Journal of Transport Geography* 12 (2) (2004) 127–140. doi:10.1016/j.jtrangeo.2003.10.005.
- [443] [16] S. L. Handy, D. A. Niemeier, Measuring accessibility: an exploration of issues and alternatives, *Environment and Planning A* 29 (7) (1997) 11751194.
- [444] [17] M. Miller, Seismic risk assessment of complex transportation networks, PhD thesis, Stanford University (2014).
- [445] [18] M. Miller, J. Baker, Ground-motion intensity and damage map selection for probabilistic infrastructure network risk assessment using optimization, in review (2014).
- [446] [19] R. Cervero, K.-L. Wu, Polycentrism, commuting, and residential location in the San Francisco Bay area, *Environment and Planning A* 29 (5) (1997) 865–886.
- [447] [20] D. M. Boore, G. M. Atkinson, Ground-motion prediction equations for the average horizontal component of PGA, PGV, and 5%-damped PSA at spectral periods between 0.01 s and 10.0 s, *Earthquake Spectra* 24 (1) (2008) 99–138.
- [448] [21] N. Abrahamson, W. Silva, Summary of the Abrahamson & Silva NGA Ground-Motion Relations, *Earthquake Spectra* 24 (1) (2008) 67–97. doi:10.1193/1.2924360.
- [449] [22] B. Chiou, R. R. Youngs, An NGA model for the average horizontal component of peak ground motion and response spectra, *Earthquake Spectra* 24 (1) (2008) 173–215. doi:10.1193/1.2894832.
- [450] [23] K. W. Campbell, Y. Bozorgnia, NGA ground motion model for the geometric mean horizontal component of PGA, PGV, PGD and 5% damped linear elastic response spectra for periods ranging from 0.01 to 10s, *Earthquake Spectra* 24 (1) (2008) 139–171. doi:10.1193/1.2857546.
- [451] [24] J. W. Baker, C. A. Cornell, Which spectral acceleration are you using?, *Earthquake Spectra* 22 (2) (2006) 293–312. doi:10.1193/1.2191540.
- [452] [25] R. Foulser-Piggott, P. J. Stafford, A predictive model for Arias intensity at multiple sites and consideration of spatial correlations, *Earthquake Engineering & Structural Dynamics* 41 (3) (2012) 431451. doi:10.1002/eqe.1137.
- [453] [26] Y. Han, R. A. Davidson, Probabilistic seismic hazard analysis for spatially distributed infrastructure, *Earthquake Engineering & Structural Dynamics* 41 (15) (2012) 2141–2158. doi:10.1002/eqe.2179.
- [454] [27] N. Jayaram, J. W. Baker, Correlation model for spatially distributed ground-motion intensities, *Earthquake Engineering & Structural Dynamics* 38 (15) (2009) 1687–1708. doi:10.1002/eqe.922.
- [455] [28] E. H. Field, T. H. Jordan, C. A. Cornell, OpenSHA: a developing community-modeling environment for seismic hazard analysis, *Seismological Research Letters* 74 (4) (2003) 406 – 419. doi:10.1785/gssrl.74.4.406.
- [456] [29] M. Shinozuka, Y. Murachi, X. Dong, Y. Zhou, M. J. Orlikowski, Effect of seismic retrofit of bridges on transportation networks, *Earthquake Engineering and Engineering Vibration* 2 (2) (2003) 169–179. doi:10.1007/s11803-003-0001-0.
- [457] [30] E. H. Field, T. E. Dawson, K. R. Felzer, A. D. Frankel, V. Gupta, T. H. Jordan, T. Parsons, M. D. Petersen, R. S. Stein, R. J. Weldon, C. J. Wills, Uniform California Earthquake Rupture Forecast, Version 2 (UCERF 2), *Bulletin of the Seismological Society of America* 99 (4) (2009) 2053 –2107. doi:10.1785/0120080049.
- [458] [31] D. J. Wald, T. I. Allen, Topographic slope as a proxy for seismic site conditions and amplification, *Bulletin of the Seismological Society of America* 97 (5) (2007) 1379–1395. doi:10.1785/0120060267.
- [459] [32] N. Basöz, J. Mander, Enhancement of the highway transportation lifeline module in HAZUS, Tech. rep., Final Pre-Publication Draft (#7) prepared for the National Institute of Building Sciences (NIBS) (1999).
- [460] [33] K. N. Ramanathan, Next generation seismic fragility curves for California bridges incorporating the evolution in seismic design philosophy, PhD thesis, Georgia Institute of Technology (2012).
- [461] [34] R. Lee, A. S. Kiremidjian, Uncertainty and correlation for loss assessment of spatially distributed systems, *Earthquake Spectra* 23 (4) (2007) 753–770. doi:10.1193/1.2791001.
- [462] [35] S. Werner, C. Taylor, S. Cho, J. Lavoie, REDARS 2 methodology and software for seismic risk analysis of highway systems (technical manual), Tech. rep., Seismic Systems & Engineering Analysis for MCEER, Oakland, CA (2006).
- [463] [36] Caltrans, Caltrans Seismic Design Criteria Version 1.7, Tech. Rep. SDC 1.7, California Department of Transportation, Sacramento, CA (2013).
- [464] [37] Bechtel/HNTB Team, Design Criteria Volume I, Version 1.2, Tech. rep., San Francisco Bay Area Rapid Transit District, San Francisco Bay Area Rapid Transit District Earthquake Safety Program (2008).
- [465] [38] N. Kurtz, J. Song, P. Gardoni, Time-varying seismic reliability analysis of representative US west coast bridge transportation networks, in: G. Deodatis, B. R. Ellingwood, D. M. Frangopol (Eds.), *Safety, Reliability, Risk and Life-Cycle Performance of Structures and Infrastructures*, CRC Press, 2014, pp. 655–662.
- [466] [39] J. Ghosh, K. Rokneddin, J. E. Padgett, L. Dueas-Osorio, Seismic reliability assessment of aging highway bridge networks with field instrumentation data and correlated failures. I: Methodology, *Earthquake Spectra* 30 (2) (2013) 795–817. doi:10.1193/040512EQS155M.
- [467] [40] S. Pugh, Construction statistics, Tech. rep., California Department of Transportation Division of Engineering Services (2012).
- [468] [41] K. Kockelman, Travel Behavior as Function of Accessibility, Land Use Mixing, and Land Use Balance: Evidence from San Francisco Bay Area, *Transportation Research Record: Journal of the Transportation Research Board* 1607 (-1) (1997) 116–125. doi:10.3141/1607-16.
- [469] [42] P. Waddell, F. Nourzad, Incorporating nonmotorized mode and neighborhood accessibility in an integrated land use and transportation model system, *Transportation Research Record: Journal of the Transportation Research Board* 1805 (-1) (2002) 119–127. doi:10.3141/1805-14.
- [470] [43] C. F. Manski, *Structural analysis of discrete data with econometric applications*, MIT Press, 1981.
- [471] [44] K. A. Small, H. S. Rosen, Applied welfare economics with discrete choice models, *Econometrica* 49 (1) (1981) 105–130. doi:10.2307/1911129.
- [472] [45] D. Ory, Personal communication (2013).
- [473] [46] United States Department of Transportation, Revised departmental guidance: valuation of travel time in economic analysis, US Department of Transportation, Washington, DC.
- [474] [47] G. Erhardt, P. Brinckerhoff, D. Ory, A. Sarvepalli, J. Freedman, J. Hood, B. Stabler, MTC's Travel Model One: applications of an activity-based model in its first year, in: *Innovations in Travel Modeling 2012*, Tampa, Florida, 2012, p. 9.
- [475] [48] P. Waddell, UrbanSim: modeling urban development for land use, transportation, and environmental planning, *Journal of the American*

- 506 Planning Association 68 (3) (2002) 297–314. doi:10.1080/01944360208976274.
- 507 [49] W. Davidson, P. Vovsha, J. Freedman, R. Donnelly, CT-RAMP family of activity-based models, in: Proceedings of the 33rd Australasian  
508 Transport Research Forum (ATRF), Canberra, Australia, 2010, p. 15.
- 509 [50] H. Wakabayashi, H. Kameda, Network performance of highway systems under earthquake effects: a case study of the 1989 Loma Prieta  
510 earthquake, in: Proceedings US-Japan Workshop on Earthquake Disaster Prevention for Lifeline Systems, 1992, pp. 215–232.
- 511 [51] U.S. Bureau of the Census, United States Census 2010, Tech. rep., U.S. Census Bureau, Washington D.C. (2010).